Lawrence Berkeley National Laboratory

Lawrence Berkeley National Laboratory

Title

Detailed modeling and laser-induced fluorescence imaging of nitric oxide in a NH(i)-seeded non-premixed methane/air flame

Permalink

https://escholarship.org/uc/item/83n5273w

Authors

Bell, John B.
Day, Marcus S.
Grcar, Joseph F.
et al.

Publication Date

2001-12-14

eScholarship.org Powered by the California Digital Library
University of California

LBNL-49333

Detailed modeling and laser-induced fluorescence imaging of nitric oxide in a NH_3-seeded non-premixed methane/air flame

John B. Bell, Marcus S. Day, Joseph F. Grcar

Computing Sciences Directorate
Lawrence Berkeley National Laboratory
Berkeley, California, 94720, USA

Wolfgang G. Bessler, Christof Schulz

University of Heidelberg
Im Neuenheimer Feld 253
69120 Heidelberg, Germany

Peter Glarborg, Anker D. Jensen

Department of Chemical Engineering
Technical University of Denmark
DK-2800, Lyngby, Denmark

This work was supported under the SciDAC Program by the Director, Office of Science, Office of Advanced Scientific Computing Research, Mathematical, Information, and Computational Sciences Division of the U.S. Department of Energy, contract No. DE-AC03-76SF00098.

Detailed modeling and laser-induced fluorescence imaging of nitric oxide in a NH_3-seeded non-premixed methane/air flame

Abstract

In this paper we study the formation of NO in laminar, nitrogen diluted methane diffusion flames that are seeded with ammonia in the fuel stream. We have performed numerical simulations with detailed chemistry as well as laser-induced fluorescence imaging measurements for a range of ammonia injection rates. For comparison with the experimental data, synthetic LIF images are calculated based on the numerical data accounting for temperature and fluorescence quenching effects. We demonstrate good agreement between measurements and computations. The LIF corrections inferred from the simulation are then used to calculate absolute NO mole fractions from the measured signal.

The NO formation in both doped and undoped flames occurs in the flame sheet. In the undoped flame, four different mechanisms contribute to NO formation. The present calculations show the most important pathway is prompt NO, followed by the NNH mechanism, thermal NO and the N_2O mechanism. As the NH_3 seeding level increases, fuel-NO becomes the dominant mechanism and N_2 shifts from being a net reactant to being a net product. Nitric oxide in the undoped flame as well as in the core region of the doped flames are underpredicted by the model; we attribute this mainly to inaccuracies in the NO recycling chemistry on the fuel-rich side of the flame sheet.

Introduction

Oxidation of fuel-bound nitrogen is the dominant source of nitric oxide in combustion of solid fuels such as coal and biomass. Most of the fuel-nitrogen is released with the volatiles during devolatilization and subsequently oxidized in gas-phase diffusion flames. Despite the importance of fuel-NO, comparatively little work has been reported on conversion of reactive nitrogen species in non-premixed flames.

Studies of laminar diffusion flames doped with fuel-N show that the species composition of gas-phase fuel-N does not have a significant effect on NO yield [20]. The major parameters for fuel-N selectivity towards NO or N_2 appear to be the fuel-N dopant level and the flame configuration. At typical fuel-N/fuel ratios of about 1%, the conversion efficiency to NO is often below 30% for non-premixed flames [20, 25]. This is remarkably lower than the values of 80–100% reported for lean premixed flames with similar fuel-N seeding amounts [14, 30]. Despite the considerable progress over the last decade in modeling laminar non-premixed flames with detailed chemistry (see

[2, 23, 24] and references therein), no study of fuel-nitrogen effects has been performed until recently.

Sullivan et al. [25] conducted a combined experimental and modeling investigation of NO_x formation in nitrogen-diluted laminar methane diffusion flames seeded with ammonia. The computations were performed with a two-dimensional model that included detailed chemical kinetics. The model showed good agreement with exhaust gas concentrations of NO over a wide range of NH_3 seeding. In particular, the declining efficiency of NH_3 to NO conversion with increased fuel-ammonia in nonpremixed flames [20] was observed both experimentally and in the simulations. Based on analysis of the calculations, the changes in NO formation and consumption mechanisms with increasing amounts of ammonia in the fuel were identified.

Even though the agreement between model and experiments in the work of Sullivan et al. is encouraging, flue data alone are insufficient for model validation. For this purpose in-flame measurements are required, providing detailed characterization of the flame structure. In the present work we combine high-resolution numerical simulations with laser-induced fluorescence (LIF) imaging measurements to study steady laminar diffusion flames with various levels of fuel-N.

The present experimental set-up involves axisymmetric laminar coflowing nonpremixed CH_4/air flames doped with NH_3, similar to those studied by Sullivan et al. The calculations are performed with a two-dimensional model [7] using the reaction mechanism proposed by Glarborg et al. [11]. The objective of this work is partly to validate the model and partly to analyze further the NO formation mechanisms in non-premixed flames doped with fuel-N.

In the following sections we describe both the experimental setup and the computational methodology used in this study. We then provide a detailed comparison between the numerical results and the measured data. Finally, we discuss how added ammonia affects the nitrogen chemistry within the flames.

Experiment

Background

Laser-induced fluorescence is frequently used as a non-intrusive technique for quantitative measurements of NO concentrations and temperatures in combustion processes. Quantitative NO-imaging has been performed in laminar [15] and turbulent [5, 17] atmospheric-pressure and high-pressure [4, 12] flames. LIF-based thermometry has been performed using the NO molecule as a temperature probe. Rotational [26] as well as vibrational [3] temperatures have been measured using one- [26], two- [3, 26] or multi-line [4, 28] techniques.

The dependence of NO-LIF intensity, I_{LIF}, for weak, non-perturbing laser excita-

tion is given by

$$I_{\mathrm{LIF}} \;=\; c_{cal}\, I_{\mathrm{laser}}\, N_{\mathrm{NO}} \sum_i f_{B,i}(T)\, B_{i,k}\; g_{\lambda,i}(p,T,X) \sum_{k,j} \frac{A_{k,j}}{\sum_\ell A_{k,\ell} + Q_k(p,T,X)}\,. \qquad (1)$$

I_{LIF} depends on the number density of the excitable molecules (number density N_{NO} times the Boltzmann fraction $f_{B,i}$), the Einstein coefficient $B_{i,k}$ for absorption $i \to k$, the spectral overlap fraction $g_{\lambda,i}(p,T,X)$ of the laser spectral profile and the NO absorption spectrum, and the fluorescence quantum yield $A/(\sum A + Q)$, where A and Q are decay rates due to spontaneous emission and electronic quenching, respectively. The summations account for overlapping transitions and rotational energy transfer in the excited state.

Q is calculated using temperature-dependent quenching cross-sections from Paul et al. [19]. The overlap fraction $g_{\lambda,i}$ is calculated using Doppler and pressure broadening as well as collisional shifting models [6, 8, 9, 29]. NO transition frequencies and rotational line strengths are calculated using relations from Paul [18], with vibrational transition probabilities from Laux and Kruger [13].

Equation 1 thus provides a quantitative relationship between I_{LIF} and the NO number density N_{NO} or mole fraction $X_{\mathrm{NO}} = N_{\mathrm{NO}}\, p/kT$. Its evaluation requires knowledge of temperature, T, and species mole fractions, X.

Temperature is measured in a two-line approach using NO excitation from different vibrational ground states [3]. The large difference in ground state energies provides high temperature sensitivity at combustion temperatures (900–3000 K). The NO transitions we use for thermometry and concentration measurements are the A-$X(0,0)$ $R_{11} + Q_{21}(21.5)$ feature at 225.25 nm and the A-$X(0,2)$ O_{12} bandhead at 247.94 nm. The choice of these transitions is governed by the availability of a tunable KrF excimer laser that can be used directly or in combination with a hydrogen Raman cell to generate the required wavelengths in the (0,0) and (0,2) band, respectively [10].

Setup

The investigations are carried out at atmospheric pressure in a modified Taran type burner [16] consisting of an inner (fuel, 1.0 cm diameter) and an outer (oxidizer, 3.25 cm diameter) tube. The reaction zone is enclosed by a fused silica tube (3.35 cm diameter) to stabilize the flame. Constant gas flows are provided by mass flow controllers (*Tylan*, *Bronkhorst*). The oxidizer is air (6.26 l/min). For the fuel flow, methane (0.103 l/min) is diluted with a nitrogen/NH_3 mixture (0.151 l/min) with various amounts of NH_3. Experimental and computational results are reported here for 0, 260, 420, 590, 790 and 1420 ppm of NH_3 in the fuel. For the temperature measurements, the fuel is seeded with 260 ppm NO (no NH_3) to yield high LIF-signal intensities in all regions of the flame.

The beam from a tunable, narrowband ($\Delta v = 0.6$ cm^{-1}) KrF excimer laser (*Lambda Physik*, EMG 150) is used to pump a Raman shift cell (H_2, 8 bar). A Pellin-Broca prism and a slit aperture separate the fundamental frequency ($\approx$ 248 nm) and the first anti-Stokes line ($\approx$ 225 nm). A cylindrical lens and aligned with the center of the flame forms each laser beam into a vertical light sheet (30×0.8 mm^2 cross-section). The laser energy is detected by a fast photodiode. LIF-signals are focused (*Nikon*, $f = 105$ mm, $f_{\#} = 4.5$) onto an intensified CCD camera (*LaVision*, StreakStar, 100 ns exposure time). Reflection bandpass filters in combination with a 248 nm short-pass filter isolate the NO (0,1) fluorescence around 236 nm from LIF signal interference and from elastically scattered light for both excitation wavelengths. The raw images are corrected for spatial and temporal laser energy fluctuations. The remaining background is corrected by taking data with the laser tuned off the NO resonance.

Calibration of both temperature and NO concentration is performed in a lean ($\phi = 0.92$) premixed ethylene/air flame. The temperature in this flame is known from CARS measurements [1]. The LIF signal is calibrated using a standard addition technique by seeding 100–1500 ppm NO into the lean premixed flame [4, 5, 27]. For correct application of this technique, a loss of 10% of the added NO due to reburn reactions in the flame front must be accounted for [15, 21, 31].

Simulation Methodology

The numerical simulations evolve a low Mach number model [7] to a steady state. The axisymmetric model includes conservation equations for species mass and total enthalpy, and incorporates a detailed chemical mechanism due to Glarborg, et al. [11], with transport properties from Sullivan et al. [25]. The numerical algorithm is based on a sequential predictor-corrector formulation, using a Godunov upwind method for advection terms, and a semi-implicit (Crank-Nicholson) treatment of diffusion. The chemical kinetics are integrated using implicit backward-difference methods. The low Mach number formulation introduces an elliptic constraint on the velocity field; a modified projection method enforces this constraint on the solution.

The simulations use an adaptive numerical grid, which increases resolution in the flame zone. This affords a large computational domain extending throughout the entire quartz tube (radius 1.675 cm, length 30.15 cm). A five-level adaptive grid hierarchy is used, where each level is a factor of two finer than the next coarser level. The finest cells (in the flame zone) are approximately 65 μm on a side. This adaptive methodology has been shown to provide accurate predictions of NO_x formation in ammonia-enriched non-premixed flames [25].

Comparison of Experiment and Simulation

Flame Height

The simulated and experimental flames show a noticeable discrepancy in height. If h_f is the height above the burner exit of the flame front in the center of the flame, we find $h_{f,exp.} = 21.5$ mm and $h_{f,sim} = 30$ mm for the flame seeded with 1420 ppm NH_3. We believe this arises from differences between conditions at the burner exit in the experiments and the boundary conditions in the simulations. The burner housing is water-cooled to 283 K which the simulations assume is also the temperature of the inflowing gases and of the burner tip. Further, the simulations assume fully developed laminar flow of the entering fuel and oxidizer, though measurements to verify this assumption are not available.

Nevertheless, the experimental and numerical flames are self-similar and the differences in the flame length do not appear to affect the chemistry. Therefore, for the remainder of the paper we scale the computational results vertically to match the experimental flame height. The resulting images shown here represent an area of 16×30 mm^2.

Temperature Fields

Figure 1 compares experimental and computed temperature fields for the flames considered here. The temperature is measured using the two-line technique [3] described in the background section with 260 ppm of NO seeded in the fuel to provide high LIF intensities throughout the flame. The vertical stripes at the sides of the flame are due to laser beam reflections on the quartz cylinder. The overall error of the LIF temperature measurement is within $\pm 5.5\%$, which corresponds to ≈ 100 K at the maximum flame temperature. This error estimate is based on experimental precision, accuracy of the CARS temperature calibration [1], and uncertainties in the NO spectroscopic data used in the two-line data reduction.

The agreement between measurement and computation is excellent. The principal differences are that the computations predict higher temperature in the lower portion of the flame and the measured temperature shows a slightly broader region of high temperature near the flame tip.

Comparison of Observed and Synthetic LIF Signals

Typically, experimental data is processed to obtain mole fractions of the quantity of interest for direct comparison to simulation results. As discussed above, conversion of the NO-LIF signal to quantitative NO mole fractions requires corrections for local

temperature and species concentrations that are only known approximately. The quenching correction is particularly delicate for nonpremixed flames [22].

On the other hand, all of the data required to compute I_{LIF} are available from the simulation except the calibration constant c_{cal} which connects $I_{\mathrm{LIF}}/I_{\mathrm{laser}}$ to a standard LIF intensity emitted from a known NO concentration at the local T and X of the calibration flame. Rather than compare processed LIF data with simulations, we compute synthetic NO-LIF images using the simulation results and compare those directly with the unprocessed LIF signals. The model then consists of both the simulation results (based on our understanding of fluid dynamics and chemical kinetics) and the fluorescence calculation (based on our understanding of NO molecular spectroscopy). The experimental data consist of the measured signal corrected for spatial variations in laser energy.

Figure 2 compares such "synthetic" LIF with the calibrated, experimental LIF images with A-X(0,0) excitation for flames with different NH_3 seeding concentrations. The over-all agreement between the measured LIF and the synthetic LIF is excellent. The simulations, however, predict a weaker signal in the lower central part of the flame, which also shows slight differences in shape. With decreasing NH_3 seeding, the simulations increasingly underpredict the measured NO-LIF signals not only in the flame center, but also in the flame sheet. Similar conclusions can be drawn from images from a higher ground state (A-X(0,2) excitation) which are not shown for reasons of space.

NO Concentration

To investigate the quantitative agreement in more detail we derive NO concentrations from the calibrated experimental NO A-X(0,0) LIF data in Fig. 2. The experimental temperatures (Fig. 1) are used for Boltzmann and overlap fraction corrections. Quenching corrections are derived from the simulated concentrations of the major species CO, CO_2, H_2O, N_2, and O_2; this approach has been used before [23], though not for fuel-N seeded flames. For relative NO concentrations the error bounds are ±9–10% depending on the position in the flame. Following a standard error propagation calculation, uncertainties in temperature, quenching rate, and the LIF experiment (laser energy, detection, image noise) contribute in approximately equal amounts. The dependence on position is due to the variation of the LIF temperature sensitivity with local temperature. The additional inaccuracy of the calibration procedure yields a total error within ±13–15% for absolute NO concentrations.

Essentially the same concentrations are obtained by using NO A-X(0,2) data (not shown here). However, signal/noise decreased because of the higher temperature sensitivity and lower signal levels, leading to an uncertainty of up to ±23% in the colder, central region of the flame.

Figure 3 displays the experimental and simulated NO concentration fields. Due to

the corrections for temperature and fluorescence quenching, the spatial distribution of NO differs from what might be anticipated by examining the LIF data in Fig. 2. In particular, the strong LIF signal in the central, cooler part of the flame observed in Fig. 2 is not actually indicative of an extremely high NO concentration.

NO concentration profiles are shown in Fig. 4. The profiles at 1 cm above the burner exit intersect the middle of the region of intense LIF signal in the lower part of the frames in Fig. 2. As already evident from the LIF images, the simulations underpredict NO concentrations in the cool center of the flame at this elevation. However, as can be seen in the right half of the figure, at higher elevations the agreement between experiment and simulation is very good for all but the lowest level of NH_3 seeding.

Discussion

Integrated Nitrogen Reaction Paths

We use integrated reaction path diagrams to summarize the nitrogen chemistry in the simulations. Fig. 5 shows how nitrogen moves through the chemical species of the flames with 0 and 1420 ppm of NH_3 seeding. The diagrams reveal the extent to which the nitrogen chemistry is quickly dominated by fuel bound nitrogen.

With no NH_3 seeding, all nitrogen chemistry stems from N_2. Due to the large range of conditions occurring in the nonpremixed flame, no less than four mechanisms contribute to NO: thermal NO (initiating in paths $N_2 \rightarrow N, NO$), prompt NO (paths $N_2 \rightarrow N, HCN$), the N_2O (path $N_2 \rightarrow N_2O$), and the NNH mechanism (path $N_2 \rightarrow NNH$). Prompt NO is most important for NO formation, with the NNH mechanism a surprising second. In the fuel-rich parts of the flame where hydrogen atoms reach high concentrations, N_2 and NNH are almost in partial equilibrium. Subsequent reactions $NNH + O \rightarrow N_2O + H$ or $NH + NO$ initiate a reaction sequence that yields significant amounts of NO.

With NH_3 added to the flame, fuel-NO becomes important. At 1420 ppm NH_3 seeding, the amine chemistry has reversed the net flow of nitrogen atoms out of molecular nitrogen, which is now a net product. In both doped and undoped flames there is considerable recycling of nitrogen through cyano species. The results are consistent with the observations of Sullivan et al. [25] who offer a detailed discussion of the nitrogen chemistry in these flames based on simulations.

Location of Peak NO Concentration

The fuel-nitrogen level affects not only the chemical mechanism for NO formation, but also the location of peak NO concentration. Thermal and prompt NO, which dominate at zero or low fuel-N levels, occur in the thin, parabola-shaped flame sheet.

As can be seen in the faint 0 ppm case of Fig. 3, NO concentrations just to the outside of the flame sheet increase with elevation leading to a peak in concentration downstream of the flame tip.

As the fuel-N seeding of the flame increases, however, the peak NO concentration spreads throughout the flame sheet (Fig. 3). Specifically, in the case of 1420 ppm NH_3 seeding, the simulation shows that a peak NO level of about 210 ppm occurs in a thin region that overlaps the parabola-shaped flame sheet. On the centerline, both peak NO and peak $T = 1810$ K occur at a height of $z = 2.1$ cm. The NO concentration drops off smoothly on the lean side of the flame as the NO mixes with other gases.

NO in the Low-Temperature Flame Center

As the LIF images show, there is also some NO inside the low-temperature flame core. This can be attributed to diffusion and convection of NO and NO_2 from the flame sheet. The small amount of NO formed inside the core is largely due to reduction of NO_2, for instance by the reaction $CO + NO_2$. In contrast, the major NO producing reaction in the flame sheet, $N + OH \rightarrow NO + H$, creates 0.26 mol/m^{3}s of NO just inside the flame tip, at $z = 2.0$ cm, and reaches as high as 2.0 mol/m^{3}s at the base of the flame sheet. This is four orders of magnitude more than any reactions that produce NO in the flame core.

The LIF images also show a very faint depletion zone for NO on the centerline. This is also indicated by the simulation. For example, for 1420 ppm NH_3 seeding, NO on the centerline has a local peak of 90 ppm at $z = 1.2$ cm, then dips to 77 ppm at $z = 1.8$ cm, before rising to 210 ppm at $z = 2.1$ cm at the flame tip. The slight drop is due to reactions such as $CH_3 + NO \rightarrow H_2CN + OH$ which occurs at the rate of about 10^{-5} mol/m^{3}s over the range from $z = 1.5$ to 1.8 cm. For perspective on the strength of this reaction, the major NO consuming reaction is $HCCO + NO \rightarrow HCN + CO_2$. This occurs along and just inside the flame sheet and peaks at 0.25 mol/m^{3}s at $z = 2.0$ cm.

Due to the low temperatures and thereby low radical levels, the reactions consuming NO in the flame core are too slow to explain the differences between the measured and simulated NO concentrations in this region (Fig. 4). We attribute the discrepancy to overpredicting the NO consumption on the fuel-rich side of the flame sheet. Some refinement of the NO recycle chemistry, in particular related to the HCCO+NO reaction, may improve the agreement between the measured and simulated NO concentrations in the low-temperature flame core, as well as the general agreement for the flames with low NH_3 seedings.

Concluding Remarks

The good agreement obtained between the experimental data and the simulations supports the present modeling approach and confirms that it is possible to describe the conversion of fuel nitrogen in laminar nonpremixed flames. Through analysis of the modeling results we can obtain a good understanding of details of the flame structure and the impact of physical and chemical parameters on the conversion selectivity of fuel nitrogen to NO or N_2. The ability to predict reliably the conversion of fuel-N as a function of process parameters in laminar nonpremixed flames is of significant interest, since there are important similarities to practical flames. This work represents a step forward towards the goal of understanding and modeling fuel-N conversion in practical combustors.

References

[1] A. Arnold, B. Lange, T. Bouché, T. Heitzmann, G. Schiff, W. Ketterle, P. Monkhouse, and J. Wolfrum. Absolute temperature fields in flames by 2D-LIF of OH using excimer lasers and CARS spectroscopy. *Ber. Bunsenges. Phys. Chem.*, 96:1388–1392, 1992.

[2] B. A. V. Bennett, C. S. McENally, L. D. Pfefferle, M. D. Smooke, and M. B. Colket. Computational and experimental study of axisymmetric coflow partially premixed ethylene/air flames. *Combust. Flame*, 127:2004–2022, 2001.

[3] W. G. Bessler, F. Hildenbrand, and C. Schulz. Two-line laser-induced fluorescence imaging of vibrational temperatures in a NO-seeded flame. *Appl. Opt.*, 40:748–756, 2001.

[4] W. G. Bessler, C. Schulz, T. Lee, D.-I. Shin, M. Hofmann, J. B. Jeffries, J. Wolfrum, and R. K. Hanson. Quantitative NO-LIF imaging in high-pressure flames. *Appl. Phys. B*, 2002. submitted.

[5] S. Böckle, J. Kazenwadel, T. Kunzelmann, and C. Schulz. Laser-diagnostic multi-species imaging in strongly swirling natural gas flames. *Appl. Phys. B*, 71:741–746, 2000.

[6] A. Y. Chang, M. D. DiRosa, and R. K. Hanson. Temperature dependence of collision broadening and shift in the NO A $\leftarrow$ X (0,0) band in the presence of argon and nitrogen. *J. Quant. Spectrosc. Radiat. Transfer*, 47:375–390, 1992.

[7] M. S. Day and J. B. Bell. Numerical simulation of laminar reacting flows with complex chemistry. *Combust. Theory Modelling*, 4:535–556, 2000.

[8] M. D. DiRosa and R. K. Hanson. Collision-broadening and -shift of NO $\gamma(0,0)$ absorption lines by H_2O, O_2, and NO at 295K. *J. Mol. Spectrosc.*, 164:97–117, 1994.

[9] M. D. DiRosa and R. K. Hanson. Collision broadening and shift of NO $\gamma(0,0)$ absorption lines by O_2 and H_2O at high temperature. *J. Quant. Spectrosc. Radiat. Transfer*, 52:515–529, 1994.

[10] T. Dreier, A. Dreizler, and J. Wolfrum. The application of a Raman-shifted tunable KrF eximer laser for laser-induced fluorescence combustion diagnostics. *Appl. Phys. B*, 55:381–387, 1992.

[11] P. Glarborg, M. U. Alzueta, K. Dam-Johansen, and J. A. Miller. Kinetic modelling of hydrocarbon/nitric oxide interactions in a flow reactor. *Combust. Flame*, 115:1–27, 1998.

[12] F. Hildenbrand, C. Schulz, J. Wolfrum, F. Keller, and E. Wagner. Laser diagnostic analysis of NO formation in a direct injection diesel engine with pump-line-nozzle and common rail injection systems. *Proc. Comb. Inst.*, 28:1137–1144, 2000.

[13] C. O. Laux and C. H. Kruger. Arrays of radiative transition probabilities for the N_2 first and second positive, NO beta and gamma, N_2^+ first negative, and O_2 Schumann-Runge band systems. *J. Quant. Spectrosc. Radiat. Transfer*, 48:9–24, 1992.

[14] R. J. Martin and N. J. Brown. Nitrous oxide formation and destruction in lean, premixed combustion. *Combust. Flame*, 80:238–255, 1990.

[15] A. V. Mokhov, H. B. Levinsky, and C. E. van der Meij. Temperature dependence of laser-induced fluorescence of nitric oxide in laminar premixed atmospheric-pressure flames. *Appl. Opt.*, 36:3233–3243, 1997.

[16] K. Müller-Dethlefs, M. Peleat, and J.-P. Taran. Temperature and hydrogen concentration measurements by CARS in an ethylene-air-bunsen flame. *Ber. Bunsenges. Phys. Chem.*, 85(9):803–807, 1981.

[17] M. Namazian, J. Kelly, and R. Schefer. Simultaneous NO and temperature imaging measurements in turbulent nonpremixed flames. *Proc. Comb. Inst.*, 25:1149–1157, 1994.

[18] P. H. Paul. Calculation of transition frequencies and rotational line strengths in the γ-bands of nitric oxide. *J. Quant. Spectrosc. Radiat. Transfer*, 57:581–589, 1997.

[19] P. H. Paul, J. A. Gray, J. L. Durant, Jr., and J. W. Thoman Jr. A model for temperature-dependent collisional quencing of NO $A^2\,\Sigma^+$. *Appl. Phys. B*, 57:249–259, 1993.

[20] A. F. Sarofim, G. C. Williams, M. Modell, and S. M. Slater. Conversion of fuel nitrogen to nitric oxide in premixed and diffusion flames. *AIChE Symp. Ser.*, 71(148):51–61, 1975.

[21] C. Schulz, V. Sick, U. Meier, J. Heinze, and W. Stricker. Quantification of NO A-X(0,2) LIF:investigation of calibration and collisional influences in high-pressure flames. *Appl. Opt.*, 38:1434–1443, 1999.

[22] V. Sick, F. Hildenbrand, and P. Lindstedt. Quantitative laser-based measuerment and detailed chemical kinetic modeling of nitric oxide concentrations in methane-air counterflow diffusion flames. *Proc. Comb. Inst.*, 27:1401–1409, 1998.

[23] M. D. Smooke, A. Ern, M. A. Tanoff, B. A. Valdati, R. K. Mohammed, D. F. Marran, and M. B. Long. Computational and experimental study of NO in an axisymmetric laminar diffusion flame. *Proc. Comb. Inst.*, 26:2161–2170, 1996.

[24] M. D. Smooke, R. E. Mitchell, and D. E. Keyes. Numerical solution of two-dimensional axisymmetric laminar diffusion flames. *Combust. Sci. Tech.*, 67:85, 1989.

[25] N. Sullivan, A. Jensen, P. Glarborg, M. S. Day, J. F. Grcar, J. B. Bell, C. Pope, and R. J. Kee. Ammonia conversion and NO_x formation in laminar coflowing nonpremixed methane-air flames. *Combust. Flame*, 2001. to appear.

[26] M. Tamura, J. Luque, J. E. Harrington, P. A. Berg, G. P. Smith, J. B. Jeffries, and D. R. Crosley. Laser-induced fluorescence of seeded nitric oxide as a flame thermometer. *Appl. Phys. B*, 66:503–510, 1998.

[27] D. D. Thomsen and N. M. Laurendeau. LIF measurements and modeling of nitric oxide concentration in atmospheric counterflow premixed flames. *Combust. Flame*, 124:350–369, 2001.

[28] A. O. Vyrodov, J. Heinze, M. Dillmann, U. E. Meier, and W. Stricker. Laser-induced fluorescence thermometry and concentration measurements on NO A-X $(0, 0)$ transitions in the exhaust gas of high pressure CH_4/air flames. *Appl. Phys. B*, 61:409–414, 1995.

[29] A. O. Vyrodov, J. Heinze, and U. E. Meier. Collisional broadening of spectral lines in the A-X (0-0) system of NO by $N_2$2, Ar, and He at elevated pressures measured by laser-induced fluorescence. *J. Quant. Spectrosc. Radiat. Transfer*, 53:277–287, 1995.

[30] J. O. L. Wendt and C. V. Sternling. Effect of ammonia in gaseous fuels on NOx emissions. *J. Air Poll. Control Ass.*, 24:1055–1058, 1974.

[31] B. A. Williams and J. W. Fleming. Comparative species concentrations in CH_4/O_2/Ar flames doped with N_2O, NO, and NO_2. *Combust. Flame*, 98:93–106, 1994.

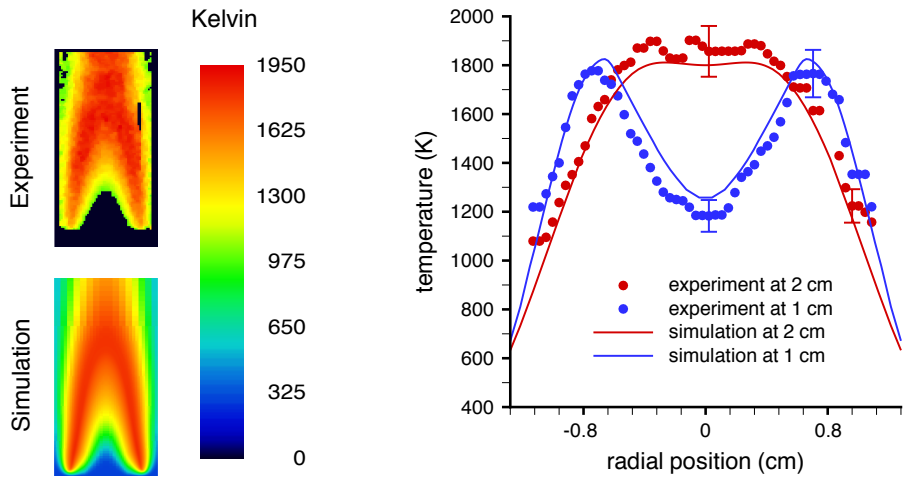

Figure 1: *Experimental and computed temperature fields. (Left) The two-dimensional region shown extends to a radius of 8 mm with a height from 0 mm to 30 mm above the nozzle exit. The experimental field is black where signal/noise was too low for evaluation. (Right) Cross-sections of the experimental and computed temperature fields at two elevations above the nozzle, 1 and 2 cm. Experimental error bars are* $\pm 5.5\%$.

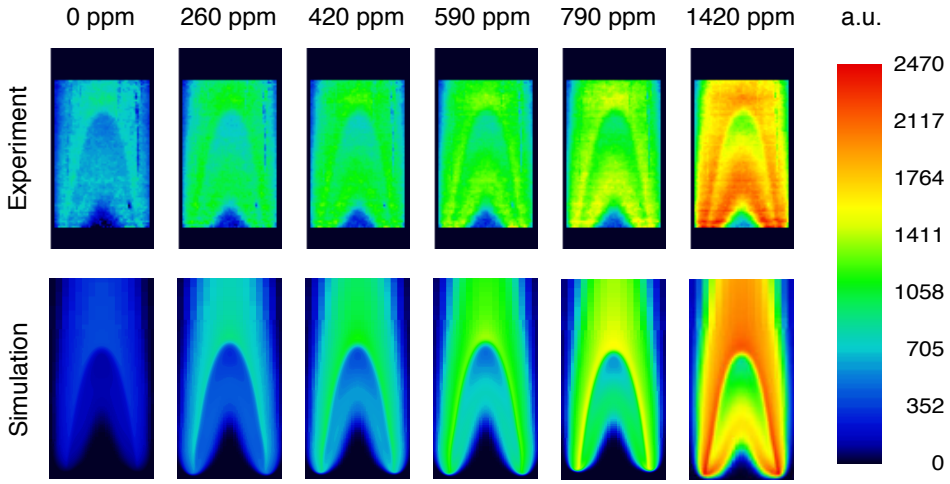

Figure 2: *NO A-X(0,0) excitation LIF images obtained (top) from measurement and (bottom) by synthetically processing the results of the flame simulation, for different* NH_3 *seeding concentrations. The experimental data and the synthetic LIF intensities are prepared independently. The color code is scaled in arbitrary units proportional to calibrated NO-LIF intensities and is identical for the simulated and the experimental images.*

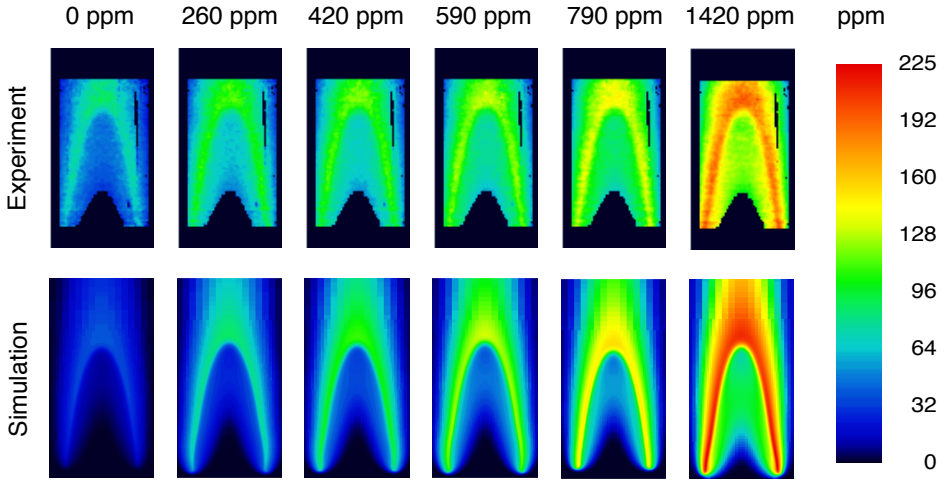

Figure 3: *Experimental and computed NO concentration fields (ppm) for various levels of NH_3 seeding in the fuel stream.*

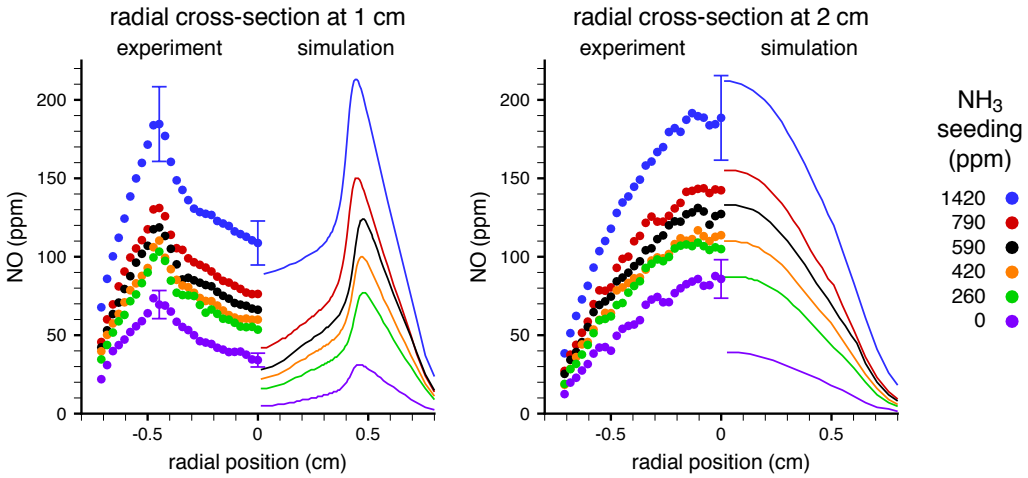

Figure 4: *Experimental and computed NO concentration profiles (ppm) at two different elevations for various levels of NH_3 seeding in the fuel stream. Experimental error is within* ±13–15% *(see text).*

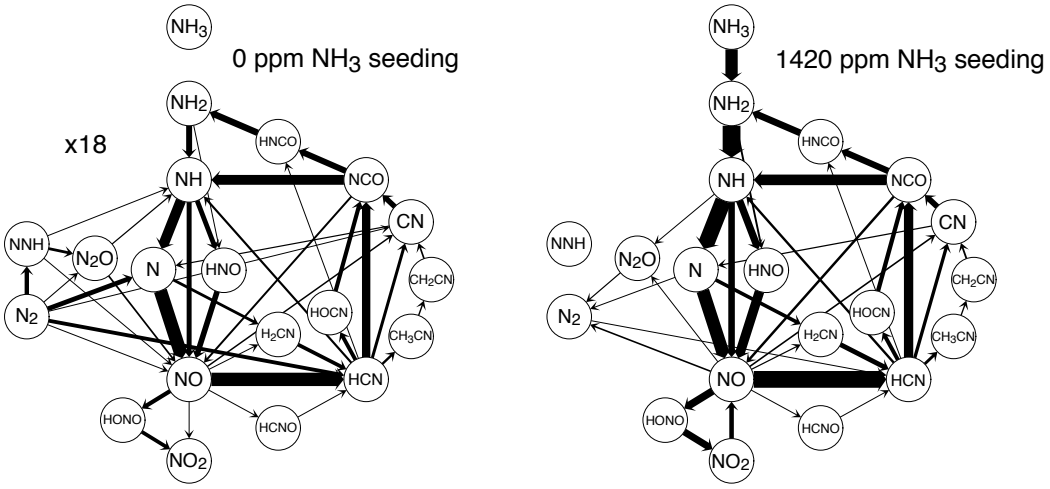

Figure 5: *Paths by which atomic nitrogen moves among the species of the flames, for the cases of no and 1420 ppm NH_3 seeding, respectively. A path's thickness indicates the net rate (mol/s) at which chemical reactions transfer nitrogen atoms between the species at its head and tail; these rates are obtained by integrating reactions' rates of progress ($mol/cm^3 s$) over the simulation domain. Nitrogen atoms are used because as a conserved scalar they provide a consistent measure of the exchange of material among species due to reaction. Only paths at least 2% of the strongest are shown. The paths in the diagram without NO seeding have been scaled by $\times 18$ to make them more visible.*